Optimal Passive Aerodynamic Control Design For Mitigating Flutter In Long-Span Bridges

Hong-Son Nguyen[1], Van-Quyen Nguyen[2], Ngoc-An Tran[3], Phan-Anh Nguyen[3*], and Ngoc-Dung Bui[4]

[1] HaUI Institute of Technology, Hanoi University of Industry, Hanoi, Vietnam
[2] Department of Mechatronics, School of Mechanical Engineering, Hanoi University of Science and Technology, Hanoi, Vietnam
[3] Faculty of Civil Engineering, Vietnam Maritime University, Haiphong City, Vietnam
[4] Faculty of Technology and Engineering, Hai Phong University, Haiphong City, Vietnam
[*] Corresponding author. E-mail: phananh.ctt@vimaru.edu.vn

Received: Jul. 29, 2025; Accepted: Nov. 06, 2025

A wide range of studies have focused on improving the aerodynamic stability of long-span bridges by raising their critical flutter wind speed. There are two main approaches to enhancing aerodynamic stability: mechanical and aerodynamic methods. The aerodynamic approach suppresses vibrations not by dissipating energy, but by generating additional aerodynamic forces induced through the installation of thin plates. However, the optimization process in the case of passive control is highly complex, as it involves not only the forces generated by wind interaction with the deck structure but also those acting on attached thin plates. This paper proposes an optimization algorithm that simplifies the determination of optimal parameters for wings used in passive aerodynamic control. Based on the complex eigenvalue method, the optimization process is implemented using the Genetic Algorithm (GA) function available in MATLAB. In addition, this paper also reviews several previously proposed passive aerodynamic control strategies and, based on that, introduces a novel configuration: a wing mounted to one side of the deck using a hinged connection and a torsional spring. Numerical simulation results demonstrate that the newly proposed configuration outperforms previous approaches in all investigated scenarios.

Keywords: Flutter; bridge deck; passive aerodynamic control; complex eigenvalue method; Genetic Algorithm

http://dx.doi.org/10.6180/jase.202607_30.009

1. Introduction

The expansion of long-span bridge construction has become increasingly prominent in modern transportation networks. Nevertheless, the aerodynamic behavior of such structures presents significant challenges, particularly as span lengths increase and structural flexibility intensifies. Wind-induced instabilities, including flutter and vortex shedding, can critically impact both the safety and functional performance of these bridges. As a result, there is a growing necessity to investigate and implement advanced methods aimed at improving aerodynamic stability.

For the phenomenon of flutter vibration, two main approaches are commonly employed: mechanical control methods and aerodynamic control methods. A typical form of mechanical control involves the application of tuned mass damping technology. The implementation of TMDs for improving the aerodynamic stability of the bridge deck is investigated with a representative bridge section, as described in previous studies [1–3]. Meanwhile, the application of multiple TMDs (MTMDs) to full bridge models has been addressed in several studies [4–6]. Another form of mechanical control involves the use of Tuned Liquid

Column Damper (TLCD). In terms of operating principle, TLCD are similar to TMD, utilizing the motion of liquid within vertical columns. However, their application has thus far been limited to enhancing the stability of structures subjected to pure torsion and harmonically varying excitation moments [7–9].

Several studies have proposed the use of passive aerodynamic appendages such as wings and flaps, with both computational and experimental results demonstrating the effectiveness of these methods. In [10], the authors investigated the placement of wings at various locations to enhance the critical wind speed, the wings can be either rigidly attached to the bridge deck or mounted onto the suspension cables. Studies [11–14] explored the installation of flaps on each side of the deck structure, with analyses conducted using both sectional and full-bridge models. In [15], a novel approach was proposed involving wings mounted under the girder in combination with a simple pendulum installed inside the bridge deck. In [16], a configuration integrating wings with torsion springs was introduced, the chosen optimization method is grid search. A novel passive aero-elastic damper for long-span bridges was presented in [17], combining small TMDs with control surfaces through a transmission mechanism. This system exploits the advantages of both TMDs and control surfaces without requiring external energy. Notably, several studies by U. Starossek have focused on rigidly attaching wings to bridge decks to enhance the critical flutter wind speed [18–21].

In general, calculating the critical flutter wind speed and solving the optimization problem for passive aerodynamic control is complex due to the wind-induced forces affecting both the bridge deck and the additional wings. In [11, 12], a minimum-state RFA (Rational Function Approximation) model of unsteady aerodynamic forces is developed using rational approximation of the generalized Theodorsen function, with a stability-based criterion for optimal control design. Nevertheless, the computational process remains highly complex and demanding. In [16], the authors employed the Step-by-Step method for estimating the critical wind speed and used the grid search method to identify the optimal parameters. However, the grid search method requires evaluation of numerous cases, and the resulting optimal values are only approximate. In this paper, the authors propose the use of complex eigenvalue method to compute the critical flutter wind speed in the case of passive aerodynamic control. Additionally, a novel approach for optimizing device parameters is introduced. The computational process is straightforward and enables rapid determination of the optimal values. The authors also extend the model presented in [16] by proposing a new control strategy involving the installation of a wing combined with a torsional spring on just one side of the deck. The concept of asymmetric damping device arrangements has been discussed in several previous studies. In [5], the wing is rigidly attached to one side of the bridge deck. In [22], the deck is equipped with an eccentric mass located on one side. In [23], a flap mounted on one side of the deck is actively controlled. In the present study, numerical simulation results demonstrate that the configuration of a wing, which is not only combined with a torsional spring but also functions as an oscillatory subsystem, placed on the leeward side of the wind flow yields superior performance compared to the other cases. However, this configuration, although more effective, is often impractical in real applications since the wind can blow from either direction. Consequently, human intervention may be required to adjust the wing position (see Fig. 1 in [10] for a possible solution).

2. Method

2.1. Analytical models of wing-bridge deck systems

This section investigates several configurations involving the attachment of wings to bridge decks. In all cases considered, the bridge deck is modeled as a sectional model with 2 degrees of freedom. The mass and mass moment of inertia per unit length of the bridge deck are denoted by m and I. The bending and torsional stiffnesses are presented by k_h and k_α, while the damping coefficients for bending and torsion are denoted by c_h and c_α. The dynamic characteristic - natural frequencies and Lehr damping - associated with bending and torsional vibrations are (ω_h, ζ_h) and $(\omega_\alpha, \zeta_\alpha)$, respectively. The shear center of the bridge deck crosssection is denoted as point S. Let B represent the width of the bridge deck. The bending and torsional displacements are represented by h and α. Wind with constant velocity U is applied to the bridge deck. The aerodynamic forces include the lift forces L_h and the moment M_α.

In this study, four aerodynamic configurations are investigated to assess their influence on the bridge deck's flutter performance.

CASE 1: Rigidly attached wings are installed on both sides of the bridge deck.

In the first case, wings of width B_w, mass per unit length m_w, and mass moment of inertia I_w (about their centroids) are rigidly attached symmetrically to the bridge deck, as depicted in Fig. 1 (**CASE 1**). The parameter e denotes the horizontal distance from each wing's centroid to the deck's shear center S. Due to the rigid attachment, the wings undergo the same rotational displacement α as the deck.

In this configuration, the dynamic equations governing the system follow a form comparable to that of a bridge

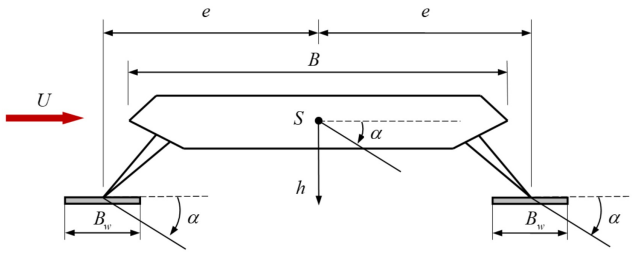

Fig. 1. Symetrical rigid attachment of wings to the bridge deck [10].

deck section [24, 25], with additional aerodynamic forces acting on the wings.

$$\begin{gathered}(m+2m_w)\,\ddot{h}+c_h\dot{h}+k_hh=L_h+L_{w1}+L_{w2}\\ \left(I+2I_w+2m_we^2\right)\ddot{\alpha}+c_\alpha\dot{\alpha}+k_\alpha\alpha=M_\alpha+M_{w1}+M_{w2}\\ -eL_{w1}+eL_{w2}\end{gathered}\tag{1}$$

These include lift forces L_{w1}, L_{w2} and moments M_{w1}, M_{w2} acting on the windward and leeward wings, respectively.

CASE 2: The wing, rigidly connected, is applied to a single side of the bridge deck.

Fig. 2 shows the second case, where only one wing is rigidly installed on the leeward side of the bridge deck (**CASE 2**). The notations used are consistent with those in **CASE 1**. The aerodynamic lift and moment acting on the wing are denoted by L_w and M_w, respectively.

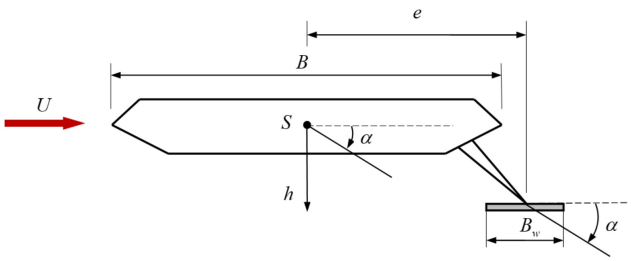

Fig. 2. A wing rigidly mounted to a single side of the bridge deck [10].

The equations of motion for this system take the following form

$$\begin{gathered}(m+m_w)\,\ddot{h}+c_h\dot{h}+k_hh=L_h+L_w\\ \left(I+I_w+m_we^2\right)\ddot{\alpha}+c_\alpha\dot{\alpha}+k_\alpha\alpha=M_\alpha+M_w+eL_w\end{gathered}\tag{2}$$

CASE 3: On each side of the bridge deck, a hinged wing with a torsional spring is mounted.

In third case, wings with the same width B_w, mass per unit length m_w, and moment of inertia per unit length I_w as in **CASE 1**. However, instead of rigid attachments, the wings are hinged to the opposite sides of the bridge deck and connected via torsional springs with stiffness k_w, as illustrated in Fig. 3 (**CASE 3**).

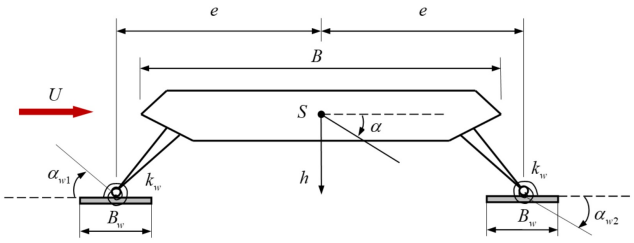

Fig. 3. Hinged attachment of wings with torsional springs on each side of the bridge deck [16].

Due to the hinged connections, the wings are allowed to rotate independently of the deck. The torsional displacements of the wings on the windward and opposite sides are denoted by α_{w1} and α_{w2}, respectively. These displacements are defined as absolute values, with their directions indicated in Fig. 3.

The governing equations for the system's motion are expressed as

$$\begin{gathered}(m+2m_w)\,\ddot{h}+c_h\dot{h}+k_hh=L_h+L_{w1}+L_{w2}\\ \left(I+2m_we^2\right)\ddot{\alpha}+c_\alpha\dot{\alpha}+(k_\alpha+2k_w)\,\alpha-\\ k_w\alpha_{w1}-k_w\alpha_{w2}=M_\alpha-eL_{w1}+eL_{w2}\\ I_w\ddot{\alpha}_{w1}-k_w\alpha+k_w\alpha_{w1}=M_{w1}\\ I_w\ddot{\alpha}_{w2}-k_w\alpha+k_w\alpha_{w2}=M_{w2}\end{gathered}\tag{3}$$

These include lift forces L_{w1}, L_{w2} and moments M_{w1}, M_{w2} acting on the windward and leeward wings, respectively.

CASE 4: Similar to **CASE 3**, but the hinged wing with torsional spring is installed only on one side of the bridge deck.

This configuration features a single wing hinged to the leeward side of the bridge deck and connected via a torsional spring, as shown in Fig. 4 (**CASE 4**). This is also the novel configuration proposed by the authors in this study. The notations used are consistent with those in **CASE 3**. The torsional displacement of the wing is denoted by α_w, and the lift force and moment acting on the wing are L_w and M_w, respectively.

The equations of motion for this configuration take the following form

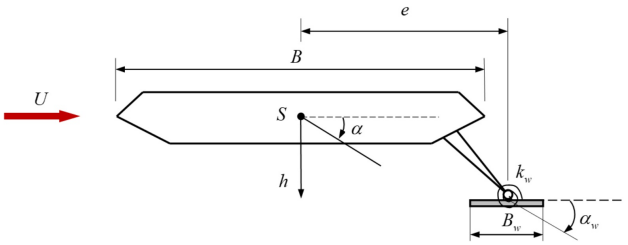

Fig. 4. Hinged attachment of a wing with torsional spring on one side of the bridge deck.

$$\begin{gathered}
\left(m+m_w\right)\ddot{h}+c_h\dot{h}+k_h h=L_h+L_w \\
\left(I+m_w e^2\right)\ddot{\alpha}+c_\alpha\dot{\alpha}+\left(k_\alpha+k_w\right)\alpha-k_w\alpha_w=M_\alpha+eL_w \\
I_w\ddot{\alpha}_w+k_w\left(\alpha_w-\alpha\right)=M_w
\end{gathered} \tag{4}$$

It can be observed that **CASE 3** is the generalized model encompassing all other cases. **CASE 1** corresponds to the scenario in which both the windward and leeward wings have sufficiently high torsional stiffness. **CASE 2** corresponds to the scenario where the windward wing has a very small width while the leeward wing still maintains sufficiently high torsional stiffness. **CASE 4** corresponds to the scenario in which the windward wing has a very small width.

The following fundamental assumptions are introduced in this study to simplify the analysis:

- The aerodynamic forces acting on the bridge deck and the wings are determined separately, without considering the aerodynamic interactions between the deck and the wings, as well as among the wings themselves, as described in [26].

- In **CASE 2** and **CASE 4**, the influence of the eccentric mass distribution is neglected.

The aerodynamic forces on the bridge deck and the wings act respectively at the shear center and the hinge points. The aerodynamic forces L_h and M_α acting on the bridge deck are expressed in real form using flutter derivatives $A_i^*, H_i^* (i = 1,2,3,4)$ [24, 25].

$$\begin{aligned}
L_h &= \frac{1}{2}\rho U^2 B\left[KH_1^*(K)\frac{\dot{h}}{U}+KH_2^*(K)\frac{B\dot{\alpha}}{U}+K^2H_3^*(K)\alpha\right. \\
&\left.+K^2H_4^*(K)\frac{h}{B}\right] \\
M_\alpha &= \frac{1}{2}\rho U^2 B^2\left[KA_1^*(K)\frac{\dot{h}}{U}+KA_2^*(K)\frac{B\dot{\alpha}}{U}+K^2A_3^*(K)\alpha\right. \\
&\left.+K^2A_4^*(K)\frac{h}{B}\right]
\end{aligned} \tag{5}$$

where U is the wind velocity and ρ is the air density.

The expression for the reduced frequency K is

$$K=\frac{\omega_F B}{U} \tag{6}$$

where ω_F is the flutter frequency.

For each bridge deck section geometry, the flutter derivatives $A_i{}^*, H_i{}^*$ are determined experimentally through wind tunnel testing. Datasets of these coefficients for typical bridge deck sections have been experimentally obtained and tabulated in [27]. In cases where the wings are modelled as thin plates, the aerodynamic loads on the plates are represented in complex form through Theodorsen's circulation functions $F(k)$ and $G(k)$ [28, 29]. The transformation of these complex force expressions into real from has been presented in [24, 25]. However, the mathematical complexity of the functions $F(k)$ and $G(k)$ poses significant challenges for the optimization process. Starossek [30] proposed empirical formulas to evaluate $F(k)$ and $G(k)$ as functions of the reduced frequency k.

$$F(k)=\frac{0.500502k^3+0.512607k^2+0.210400k+0.021573}{k^3+1.035378k^2+0.251293k+0.021508} \tag{7}$$

$$G(k)=\frac{0.000146k^3+0.122397k^2+0.327214k+0.001995}{k^3+2.481481k^2+0.934530k+0.089318} \tag{8}$$

The expression for the reduced frequency k is

$$k=\frac{\omega_F B_w}{2U} \tag{9}$$

The graphs showing the variation of Theodorsen's functions $F(k)$ and $G(k)$, calculated according to Eqs. (7) and (8), are presented in Fig. 5.

Therefore, the coefficients appearing in the aerodynamic force expressions for both the bridge deck and the wings are governed by the reduced frequencies K and k, and are ultimately determined by the flutter frequency ω_F and the flow velocity U. It should be noted that, from Eqs. (6) and (9), the quantities K and k are geometrically related and are therefore not independent variables.

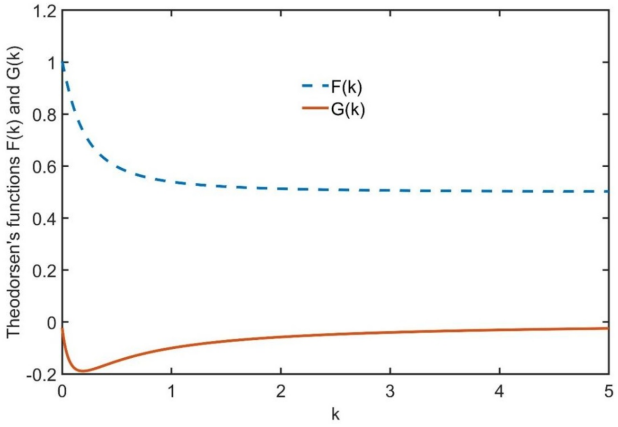

Fig. 5. Variation of Theodorsen's functions with respect to k.

2.2. Analysis based on the complex eigenvalue method

This section demonstrates the use of the complex eigenvalue method [30, 31] to evaluate the critical flutter wind speed corresponding to the configurations introduced in Section 2.1. The vibrations are assumed to be harmonic and represented in complex form, the motion equations for four cases outlined in Section 2.1 can be expressed in the following form.

$$\mathbf{M}\ddot{\mathbf{x}} + \mathbf{K}^d\mathbf{x} = \mathbf{f}_L^* \tag{10}$$

where $\mathbf{x}$ is the displacement vector, $\mathbf{M}$ is the mass matrix, $\mathbf{K}^d$ is the stiffness-damping matrix, and $\mathbf{f}_L^*$ is the generalized force vector.

For **CASE 1**, we have

$$\mathbf{x} = \begin{bmatrix} h \\ \alpha \end{bmatrix}; \mathbf{f}_L^* = \begin{bmatrix} L_h + L_{w1} + L_{w2} \\ M_\alpha + M_{w1} + M_{w2} - eL_{w1} + eL_{w2} \end{bmatrix};$$
$$\mathbf{M} = \begin{bmatrix} m + 2m_w & 0 \\ 0 & I + 2I_w + 2m_w e^2 \end{bmatrix};$$
$$\mathbf{K}^d = \begin{bmatrix} k_h + i\omega c_h & 0 \\ 0 & k_\alpha + i\omega c_\alpha \end{bmatrix} \tag{11}$$

For **CASE 2**, we have

$$\mathbf{x} = \begin{bmatrix} h \\ \alpha \end{bmatrix}; \mathbf{f}_L^* = \begin{bmatrix} L_h + L_w \\ M_\alpha + M_w + eL_w \end{bmatrix};$$
$$\mathbf{M} = \begin{bmatrix} m + m_w & 0 \\ 0 & I + I_w + m_w e^2 \end{bmatrix}; \tag{12}$$
$$\mathbf{K}^d = \begin{bmatrix} k_h + i\omega c_h & 0 \\ 0 & k_\alpha + i\omega c_\alpha \end{bmatrix}$$

For **CASE 3**, we have

$$\mathbf{x} = \begin{bmatrix} h \\ \alpha \\ \alpha_{w1} \\ \alpha_{w2} \end{bmatrix}; \mathbf{f}_L^* = \begin{bmatrix} L_h + L_{w1} + L_{w2} \\ M_\alpha - eL_{w1} + eL_{w2} \\ M_{w1} \\ M_{w2} \end{bmatrix};$$
$$\mathbf{M} = \begin{bmatrix} m + 2m_w & 0 & 0 & 0 \\ 0 & I + 2m_w e^2 & 0 & 0 \\ 0 & 0 & I_w & 0 \\ 0 & 0 & 0 & I_w \end{bmatrix};$$
$$\mathbf{K}^d = \begin{bmatrix} k_h + i\omega c_h & 0 & 0 & 0 \\ 0 & k_\alpha + 2k_w + i\omega c_\alpha & -k_w & -k_w \\ 0 & -k_w & k_w & 0 \\ 0 & -k_w & 0 & k_w \end{bmatrix} \tag{13}$$

For **CASE 4**, we have

$$\mathbf{x} = \begin{bmatrix} h \\ \alpha \\ \alpha_w \end{bmatrix}; \mathbf{f}_L^* = \begin{bmatrix} L_h + L_w \\ M_\alpha + eL_w \\ M_w \end{bmatrix};$$
$$\mathbf{M} = \begin{bmatrix} m + m_w & 0 & 0 \\ 0 & I + m_w e^2 & 0 \\ 0 & 0 & I_w \end{bmatrix}; \tag{14}$$
$$\mathbf{K}^d = \begin{bmatrix} k_h + i\omega c_h & 0 & 0 \\ 0 & k_\alpha + k_w + i\omega c_\alpha & -k_w \\ 0 & -k_w & k_w \end{bmatrix}$$

The solution toEq. (10) sought in the form:

$$\mathbf{x} = \mathbf{x}_0 e^{i\omega_F t} \tag{15}$$

where $\mathbf{x}_0$ is vibration amplitude vector.

In this formulation, the function $\mathbf{f}_L{}^*$ is expressed as

$$\mathbf{f}_L^* = \omega_F^2 \mathbf{L}^* \mathbf{x} \tag{16}$$

where $\mathbf{L}^*$ is the aerodynamic force coefficient matrix.

Eq. (10) is then rewritten in the form:

$$\left\{\mathbf{K}^d - \omega_F^2 \left[\mathbf{M} + \mathbf{L}^*\right]\right\} \mathbf{x}_0 = 0 \tag{17}$$

The condition for non-trivial solutions to Eq. (17) is that the determinant of the coefficient matrix must be equal to zero. By separating the real and imaginary parts, two nonlinear equations are obtained, corresponding to the two unknowns ω_F and U. For **CASE 1** and **CASE 2** , these equations can be solved to determine the flutter frequency ω_F and the critical flutter wind speed U_{cr}. For **CASE 3** and **CASE 4**, if the value k_w is specified, the corresponding flutter frequency ω_F and critical flutter wind speed U_{cr} can also be determined. Eq. (17) is solved using the fsolve function in MATLAB. Initial approximations are taken from the critical flutter wind speed and flutter frequency of the bridge deck without wing installation, and with this choice of initial approximations, the solutions converge.

2.3. Optimization procedure

As previously discussed, in **CASE 1** and **CASE 2**, the rigid connection between the wings and the bridges deck allows the flutter frequency ω_F and the associated wind speed U_{cr} to be directly calculated for a specified wing configuration, including size and position. In **CASE 3** and **CASE 4**, however, the torsional spring stiffness k_w is an unknown parameter. Therefore, the problem is formulated as an optimization task to determine the optimal value of k_w that maximizes the critical flutter wind speed.

The variables involved in the optimization problem are defined as follows

$$\mathbf{y} = \begin{bmatrix} y(1) & y(2) & y(3) \end{bmatrix}^T = \begin{bmatrix} \omega_F & U_{cr} & k_w \end{bmatrix}^T \quad (18)$$

Accordingly, the optimization problem can be stated as the task of finding the variable $\mathbf{y}$ that satisfies a given objective function

$$f_{\text{objective}}(\mathbf{y}) = -y(2) = -U_{cr} \rightarrow \min \quad (19)$$

Two equations derived from the determinant condition, as discussed in Section 2.2, serve as equality constraints.

Meanwhile, the inequality constraint is expressed as

$$U_{red} = \frac{U(2\pi)}{\omega_F B} = \frac{y(2)(2\pi)}{y(1)B} \leq U_{red}^{\max} \quad (20)$$

where $U_{\text{red}}^{\max}$ represents the maximum reduced wind speed within the experimental domain [27].

Using this formulation, the optimization is performed with the Genetic Algorithm (GA) implemented in the MATLAB Optimization Toolbox to determine the optimal torsional stiffness ${k_{xw}}^{opt}$ that maximizes the critical flutter wind speed. The GA is configured with a population size of 50 , a crossover rate of 0.8 , a mutation rate of 1 , and a termination criterion of 200 iterations.

3. Results and discussion

3.1. Great Belt bridge model

The cross-sectional model of the Great Belt Bridge was considered with parameters as specified in [2, 16], and these parameters are presented in Table 1. The flutter derivatives of the Great Belt bridge cross-section were determined experimentally, as reported in [27], and are illustrated in Figs. 6 and 7. It should be noted that $U_{\text{red}}^{\max}$ in [27] is equal to 16.798.

These flutter derivatives are approximated by cubic polynomial functions of the reduced speed U_{red}, as described in [2, 16]:

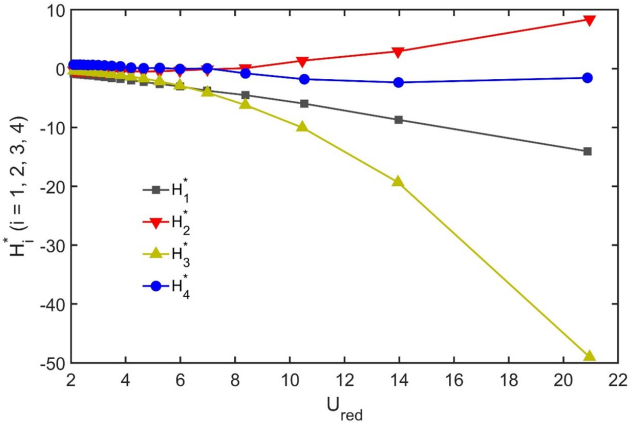

Fig. 6. Experimental values $H_i^*(i = 1, 2, 3, 4)$ with respect to U_{red} [27].

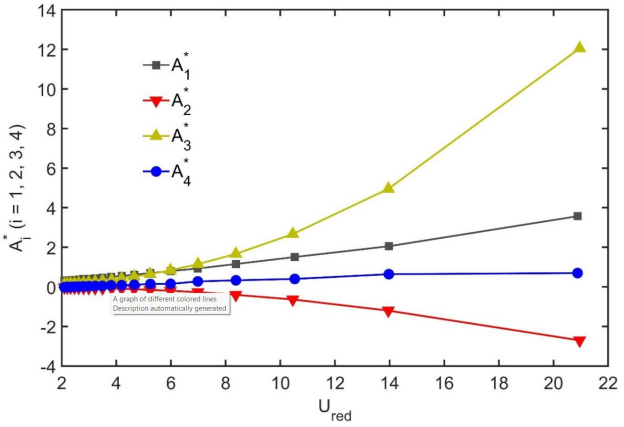

Fig. 7. Experimental values $A^*{}_i(i = 1, 2, 3, 4)$ with respect to U_{red} [27].

$$\begin{aligned}
A_1^* &= 5.3 \times 10^{-5} U_{red}^3 + 0.0016 U_{red}^2 + 0.11 U_{red} + 0.058 \\
A_2^* &= 3.6 \times 10^{-5} U_{red}^3 - 0.0076 U_{red}^2 + 0.017 U_{red} - 0.03 \\
A_3^* &= 0.00027 U_{red}^3 + 0.022 U_{red}^2 - 0.014 U_{red} + 0.066 \\
A_4^* &= -0.00018 U_{red}^3 + 0.0046 U_{red}^2 + 0.02 U_{red} - 0.069 \\
H_1^* &= 0.00032 U_{red}^3 - 0.019 U_{red}^2 - 0.42 U_{red} + 0.1 \\
H_2^* &= -0.00075 U_{red}^3 + 0.053 U_{red}^2 - 0.4 U_{red} + 0.32 \\
H_3^* &= -0.0015 U_{red}^3 - 0.086 U_{red}^2 + 0.11 U_{red} - 0.21 \\
H_4^* &= 0.002 U_{red}^3 - 0.052 U_{red}^2 + 0.13 U_{red} + 0.59
\end{aligned} \quad (21)$$

The critical flutter wind speed without the installation of wings was determined to be 40.1 m/s.

3.2. Grid search optimization

A preliminary investigation was conducted using the grid search method [32, 33] to identify the optimal torsional

Table 1. Bridge deck and wing parameters.

Parameter	Symbol	Value	Unit
Bridge deck width	B	31	m
Bridge deck mass per unit length	m	17.8×10^3	kg/m
Bridge deck mass moment of inertia per unit length	I	2.173×106	kgm^2/m
Natural frequencies	ω_h	0.62	rad/s
	ω_α	1.17	rad/s
Lehr's damping ratios	ζ_h	0	
	ζ_α	0	
Air density	ρ	1.225	kg/m^3
Wing density	ρ_w	7850	kg/m^3
Wing thickness	d	2	cm

spring stiffness ${k_w}^{\text{opt}}$ for **CASE 3** and **CASE 4**. The study assumed a ratio $2e/B = 1$ and the wing width $B_w = 0.1B$. The stiffness k_w was varied within the range $[3000 - 336000]$ Nm/rad/m with an increment step $\Delta k_w =$ 3000Nm/rad/m [16]. The results are presented in Fig. 8. It was observed that, for both **CASE 3** and **CASE 4**, optimal peaks of critical flutter wind speed exist. For **CASE 3**, the optimal ${k_w}^{\text{opt}}$ was found to be 33000Nm/rad/m corresponding to a critical flutter wind speed of 58 m/s. For **CASE 4**, the optimal ${k_w}^{\text{opt}}$ was 63000Nm/rad/m with a corresponding critical flutter wind speed of 77 m/s. It is noteworthy that as k_w increases sufficiently, a break-even condition is reached where the critical flutter wind speed equals that of the case with the wings rigidly attached to the bridge deck. For **CASE 1**, the critical flutter wind speed was 44.4 m/s, and for **CASE 2**, it was 48.2 m/s.

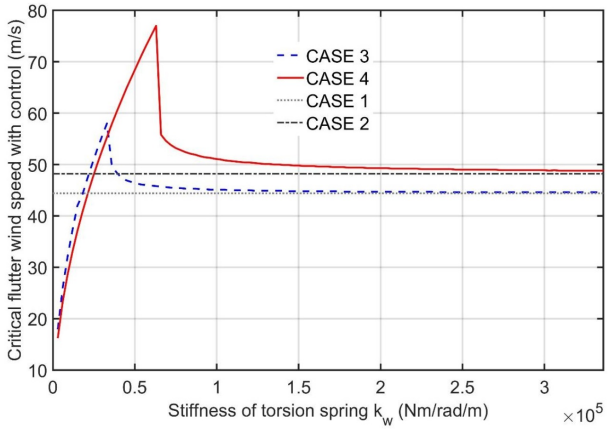

Fig. 8. Critical flutter wind speed by various values of k_w.

By employing the grid search method, a preliminary estimate of the optimal value of k_w can be obtained. From the response curves shown in Fig. 8, it is clear that k_w has an optimal value corresponding to the maximum critical flutter wind speed U_{ck}. However, the grid search method is computationally expensive, and the resulting optimal value is not entirely accurate, as it depends on the increment step Δk_w. Therefore, in the following part of this section, the optimization method presented in Section 2.3 will be applied to accurately determine the optimal torsional stiffness k_w.

3.3. Genetic algorithm optimization

The case with the ratio of $2e/B = 1$ is considered, and various B_w/B ratios are investigated. These ratios are referenced from [18]. The critical flutter wind speeds for **CASE 1**, **CASE 2** and **CASE 3**, **CASE 4** (corresponding to the optimal torsional spring stiffness values, k_w^{opt}) are presented in Table 2 and Fig. 9. The optimal values of k_w for **CASE 3** and **CASE 4** are calculated as presented in Section 2.3. It is observed that, for the case $B_w/B = 0.1$, the critical flutter wind speed obtained using the proposed optimization method is higher than or equal to that of **CASE 3** and **CASE 4** calculated using the grid search method. This indicates that the optimization approach proposed in this study yields faster and more accurate results compared to the gridbased method previously applied in [16]. Additionally, it is also observed that **CASE 4** yields the highest performance, whereas **CASE 1** provides the lowest. Configurations utilizing hinged wings with torsional springs demonstrate greater effectiveness than rigid connections. In addition, better aerodynamic efficiency is achieved when the wings are mounted only on the leeward side of the bridge deck, rather than symmetrically on both sides.

In **CASE 3** and **CASE 4**, since the wings move independently from the bridge deck, it is necessary to examine the appropriateness of the wing rotation angles. Table 3 presents the amplitude ratios between the wing rotation angles and the bridge deck rotation angles, along with the corresponding flutter frequencies. The symbols α_{0w1} and α_{0w2} denote the vibration amplitudes of the windward and leeward wings relative to the wind flow in **CASE 3**, while α_{0w} represents the vibration amplitude of the leeward wing in **CASE 4**. It is observed that for small wing widths, the torsional spring stiffness is low, resulting in

Table 2. Critical flutter wind speeds in the cases corresponding to $2e/B = 1.00$.

B_W/B	CASE 1	CASE 2	CASE 3		CASE 4	
	U_{CK} (m/s)	U_{CK} (m/s)	$k_w{}^{opt}$ (Nm/rad/m)	U_{cr} (m/s)	$k_w{}^{\mathrm{opt}}$ (Nm/rad/m)	U_{cr} (m/s)
0.025	42.0	42.8	1548	50.8	1894	54.9
0.035	42.5	43.7	3253	52.5	4269	58.6
0.045	42.9	44.5	5698	54.0	8003	62.2
0.055	43.3	45.2	8943	55.2	13233	65.2
0.065	43.6	46.0	13073	56.4	20288	68.0
0.075	43.9	46.6	18125	57.4	29321	70.6
0.085	44.1	47.3	24146	58.4	40679	73.1
0.095	44.3	47.9	31220	59.3	54731	75.7
0.100	44.4	48.2	35162	59.7	63031	77.0
0.110	44.5	48.7	43769	60.4	81734	79.5
0.120	44.7	49.3	53712	61.2	103777	81.9
0.130	44.8	49.8	64710	61.9	129741	84.3
0.140	44.9	50.3	76757	62.5	159498	86.6
0.150	45.0	50.7	90179	63.1	193235	88.8
0.160	45.1	51.2	104933	63.7	232134	91.1
0.170	45.2	51.6	120813	64.2	275823	93.3

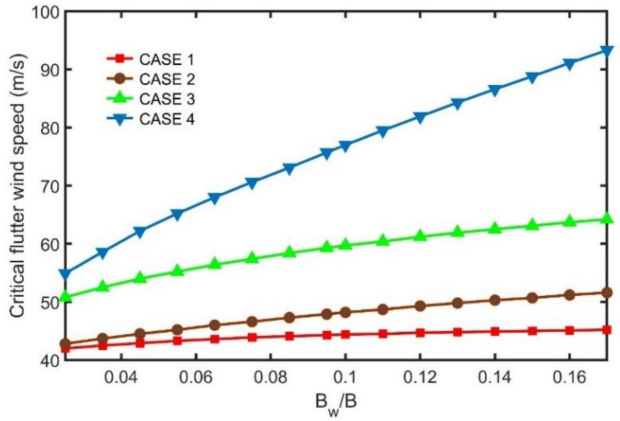

Fig. 9. Critical flutter wind speeds in the cases corresponding to the B_W/B ratios ($2e/B = 1.00$).

large amplitude ratios between the wings and the bridge deck. This amplitude ratio decreases as the wing width increases and the torsional spring stiffness rises. In **CASE 3**, the amplitude ratio of the leeward wing is larger than that of the windward wing. In contrast, for **CASE 4**, the torsional spring stiffness is higher for all wing widths, and the amplitude ratios are smaller compared to **CASE 3**.

In all four investigated cases, the wings are attached to the bridge deck through struts. In **CASE 3** and **CASE 4**, the wings are connected to the struts via a hinge located at the mid-chord, allowing them to perform independent pitching motions. The aerodynamic forces acting on the wings are transmitted to the bridge deck through the struts. The objective of the aerodynamic control is to adjust the phase angle of the wing motion such that the resulting aerodynamic forces provide positive aerodynamic damping, thereby suppressing the bridge deck vibrations. **CASE 3** and **CASE 4** exhibit better performance, as the stiffness parameters can be tuned to achieve an appropriate phase angle of wing motion. Moreover, **CASE 4** yields the best performance, despite its asymmetric configuration, because the single-sided wing arrangement allows for a more favorable adjustment of the phase angle, resulting in the most effective generation of positive aerodynamic damping.

Fig. 10 presents the optimal stiffness values (k_w^{opt}) of the torsion spring. As the wings become larger, $k_w{}^{\mathrm{opt}}$ correspondingly increases. Among the considered cases, the optimal stiffness in **CASE 4** is consistently higher than in **CASE 3**. In general, the k_w^{opt} values differ significantly, highlighting the necessity of employing an optimization algorithm to accurately determine the required values.

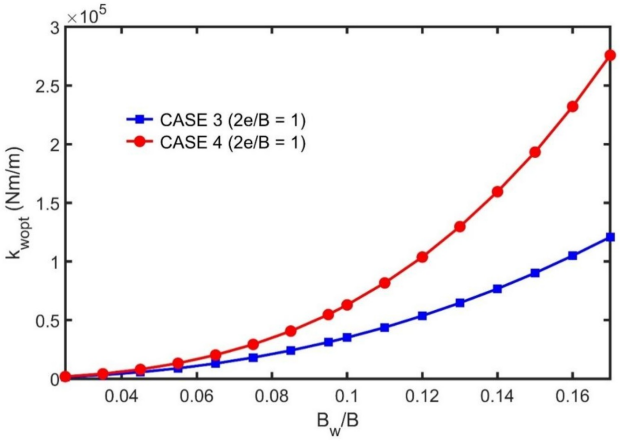

Fig. 10. Optimal values of k_{xw}^{opt} for different cases.

Table 3. Flutter frequencies and vibration amplitude ratios.

B_w/B	CASE 3			CASE 4	
	ω_F (rad/s)	α_{0wl}/α_0	α_{0w2}/α_0	ω_F (rad/s)	α_{0w}/α_0
0.025	1.0056	15.29	21.64	1.1273	11.51
0.035	1.0254	13.04	18.73	1.1886	10.17
0.045	1.0460	11.77	17.02	1.2538	9.25
0.055	1.0532	10.21	14.91	1.3109	8.46
0.065	1.0648	9.33	13.68	1.3577	7.73
0.075	1.0676	8.32	12.28	1.4071	7.21
0.085	1.0765	7.77	11.50	1.4521	6.75
0.095	1.0797	7.15	10.62	1.5056	6.45
0.100	1.0789	6.82	10.15	1.5246	6.25
0.110	1.0778	6.27	9.36	1.5722	5.97
0.120	1.0779	5.82	8.72	1.6178	5.73
0.130	1.0787	5.47	8.22	1.6618	5.50
0.140	1.0789	5.17	7.78	1.7066	5.32
0.150	1.0771	4.87	7.34	1.7513	5.16
0.160	1.0759	4.61	6.97	1.7979	5.03
0.170	1.0731	4.36	6.60	1.8416	4.90

4. Conclusions

This paper presents a range of passive aerodynamic control strategies designed to improve the critical flutter wind speed of long-span bridges. An optimization approach is employed to identify the optimal configuration of control devices that yields the maximum enhancement in critical wind speed. The optimization process is fully implemented using the Genetic Algorithm (GA) function in MATLAB and is applicable to other passive aerodynamic control methods. Additionally, a novel control measure is proposed, involving the installation of the wing on the leeward side of the bridge deck, connected via the hinge and the torsional spring. Numerical simulation results demonstrate the superior effectiveness of this approach. The influence of the size of the wings is also investigated. For CASE 3 and CASE 4, to evaluate the motion compatibility of the wings, the amplitude ratios between the wings and the bridge deck were examined for various wing widths, each associated with its corresponding optimal torsional stiffness. As the wing width increases, the optimal torsional stiffness also increases. Although the mass ratio becomes larger, the critical wind speed improves, and the amplitude ratios between the wings and the bridge deck decrease. In CASE 3, the amplitude ratio of the leeward wing is greater than that of the windward wing. In CASE 4, despite its structural asymmetry—which may require human intervention for practical implementation—the enhancement in critical wind speed is more significant than in CASE 3, and the amplitude ratio between the wing and the bridge deck is also smaller. The findings presented in this study can be further extended to active control methods and applied to full-bridge model. In the present study, the static unbalance terms have not been considered; a future research direction will focus on investigating the effects of mass eccentricity.

Acknowledgements

This research was supported by Vietnam Maritime University.

Appendix

In this section, the expressions of $\mathbf{L}^*$ for different cases are presented. First, the aerodynamic forces acting on the bridge deck can be reformulated as [30, 31].

$$L_h = \omega_F^2 \pi \rho b^2 \left(c_{hh} h + b c_{h\alpha} \alpha\right) \tag{22}$$

$$M_\alpha = \omega_F^2 \pi \rho b^2 \left(b c_{\alpha h} h + b^2 c_{\alpha\alpha} \alpha\right) \tag{23}$$

where

$$b = \frac{B}{2} \tag{24}$$

and

$$\begin{aligned} c_{hh} &= \frac{2}{\pi}\left(H_4^* + iH_1^*\right); \quad c_{h\alpha} = \frac{4}{\pi}\left(H_3^* + iH_2^*\right); \\ c_{\alpha h} &= \frac{4}{\pi}\left(A_4^* + iA_1^*\right); \quad c_{\alpha\alpha} = \frac{8}{\pi}\left(A_3^* + iA_2^*\right) \end{aligned} \tag{25}$$

- **CASE 1:** The aerodynamic forces acting on the wings are expressed as

$$\begin{aligned} L_{w1} = &\frac{1}{2}\rho U^2 B_w \left[K_w H_{w1}^*\left(K_w\right)\frac{\dot{h}_{w1}}{U} + K_w H_{w2}^*\left(K_w\right)\frac{B_w\dot{\alpha}}{U}\right. \\ &\left. + K_w^2 H_{w3}^*\left(K_w\right)\alpha + K_w^2 H_{w4}^*\left(K_w\right)\frac{h_{w1}}{B_w}\right] \end{aligned} \tag{26}$$

$$M_{w1} = \frac{1}{2}\rho U^2 B_w^2 \left[K_w A_{w1}^*(K_w)\frac{\dot{h}_{w1}}{U} + K_w A_{w2}^*(K_w)\frac{B_w\dot{\alpha}}{U} + K_w^2 A_{w3}^*(K_w)\alpha + K_w^2 A_{w4}^*(K_w)\frac{h_{w1}}{B_w}\right] \tag{27}$$

$$L_{w2} = \frac{1}{2}\rho U^2 B_w \left[K_w H_{w1}^*(K_w)\frac{\dot{h}_{w2}}{U} + K_w H_{w2}^*(K_w)\frac{B_w\dot{\alpha}}{U} + K_w^2 H_{w3}^*(K_w)\alpha + K_w^2 H_{w4}^*(K_w)\frac{h_{w2}}{B_w}\right] \tag{28}$$

$$M_{w2} = \frac{1}{2}\rho U^2 B_w^2 \left[K_w A_{w1}^*(K_w)\frac{\dot{h}_{w2}}{U} + K_w A_{w2}^*(K_w)\frac{B_w\dot{\alpha}}{U} + K_w^2 A_{w3}^*(K_w)\alpha + K_w^2 A_{w4}^*(K_w)\frac{h_{w2}}{B_w}\right] \tag{29}$$

where

$$K_w = \frac{\omega_F B_w}{U} \tag{30}$$

From Eq. (9), it follows that

$$K_w = 2k \tag{31}$$

In the case where the wings are considered as thin plates, we have [24, 25]:

$$\begin{aligned} &H_{w1}^*(K_w) = -\frac{\pi}{k}F(k);\ H_{w2}^*(K_w) = -\frac{\pi}{4k}\left[1 + F(k) + \frac{2G(k)}{k}\right];\\ &H_3^* = -\frac{\pi}{2k^2}\left[F(k) - \frac{kG(k)}{2}\right];\ H_{w4}^*(K_w) = \frac{\pi}{2}\left[1 + \frac{2G(k)}{k}\right]\\ &A_{w1}^*(K_w) = \pi\frac{F(k)}{4k};\ A_{w2}^*(K_w) = \frac{-\pi}{16k}\left[1 - F(k) - \frac{2G(k)}{k}\right];\\ &A_{w3}^*(K_w) = \frac{\pi}{8k^2}\left[\frac{k^2}{8} + F(k) - \frac{kG(k)}{2}\right];\ A_{w3}^*(K_w) = -\pi\frac{G(k)}{4k} \end{aligned} \tag{32}$$

Reformulation of the aerodynamic forces acting on the wings

$$L_{w1} = \omega_F^2\pi\rho b_w^2\left(c_{hh}^w h_{w1} + b_w c_{h\alpha}^w\alpha\right) \tag{33}$$

$$M_{w1} = \omega_F^2\pi\rho b_w^2\left(b_w c_{\alpha h}^w h_{w1} + b_w^2 c_{\alpha w\alpha w}\alpha\right) \tag{34}$$

$$L_{w2} = \omega_F^2\pi\rho b_w^2\left(c_{hh}^w h_{w2} + b_w c_{h\alpha}^w\alpha\right) \tag{35}$$

$$M_{w2} = \omega_F^2\pi\rho b_w^2\left(b_w c_{\alpha h}^w h_{w2} + b_w^2 c_{\alpha\alpha}^w\alpha\right) \tag{36}$$

where

$$b_w = \frac{B_w}{2} \tag{37}$$

and

$$\begin{aligned} &c_{hh}^w = \frac{2}{\pi}\left(H_{w4}^* + iH_{w1}^*\right);\quad c_{h\alpha}^w = \frac{4}{\pi}\left(H_{w3}^* + iH_{w2}^*\right);\\ &c_{\alpha h}^w = \frac{4}{\pi}\left(A_{w4}^* + iA_{w1}^*\right);\quad c_{\alpha\alpha}^w = \frac{8}{\pi}\left(A_{w3}^* + iA_{w2}^*\right) \end{aligned} \tag{38}$$

Note that the notations used in Eq. (38) are adopted for the remaining three cases. On the other hand, we have

$$h_{w1} = h - e\alpha;\quad h_{w2} = h + e\alpha \tag{39}$$

Thus, from Eqs. (11) and (16), it follows that

$$\mathbf{L}^* = \pi\rho\begin{bmatrix} L_{11}^* & L_{12}^* \\ L_{21}^* & L_{22}^* \end{bmatrix} \tag{40}$$

where

$$\begin{aligned} L_{11}^* &= b^2 c_{hh} + 2b_w^2 c_{hh}^w\\ L_{12}^* &= b^3 c_{h\alpha} + 2b_w^3 c_{h\alpha}^w\\ L_{21}^* &= b^3 c_{\alpha h} + 2b_w^3 c_{\alpha h}^w\\ L_{22}^* &= b^4 c_{\alpha\alpha} + 2b_w^4 c_{\alpha\alpha}^w + 2e^2 b_w^2 c_{hh}^w \end{aligned} \tag{41}$$

- **CASE 2:** By applying a similar procedure as in **CASE 1**, with

$$\mathbf{L}^* = \pi\rho\begin{bmatrix} L_{11}^* & L_{12}^* \\ L_{21}^* & L_{22}^* \end{bmatrix} \tag{42}$$

In this case, we have

$$\begin{aligned} L_{11}^* &= b^2 c_{hh} + b_w^2 c_{hh}^w\\ L_{12}^* &= b^3 c_{h\alpha} + eb_w^2 c_{hh}^w + b_w^3 c_{h\alpha}^w\\ L_{21}^* &= b^3 c_{\alpha h} + b_w^3 c_{\alpha h}^w + eb_w^2 c_{hh}^w\\ L_{22}^* &= b^4 c_{\alpha\alpha} + eb_w^3 c_{\alpha h}^w + b_w^4 c_{\alpha\alpha}^w + e^2 b_w^2 c_{hh}^w + eb_w^3 c_{h\alpha}^w \end{aligned} \tag{43}$$

- **CASE 3:** The aerodynamic forces acting on the wings are expressed as follows

$$L_{w1} = \frac{1}{2}\rho U^2 B_w \left[K_w H_{w1}^*(K_w)\frac{\dot{h}_{w1}}{U} + K_w H_{w2}^*(K_w)\frac{B_w\dot{\alpha}_{w1}}{U} + K_w^2 H_{w3}^*(K_w)\alpha_{w1} + K_w^2 H_{w4}^*(K_w)\frac{h_{w1}}{B_w}\right] \tag{44}$$

$$M_{w1} = \frac{1}{2}\rho U^2 B_w^2 \left[K_w A_{w1}^*(K_w)\frac{\dot{h}_{w1}}{U} + K_w A_{w2}^*(K_w)\frac{B_w\dot{\alpha}_{w1}}{U} + K_w^2 A_{w3}^*(K_w)\alpha_{w1} + K_w^2 A_{w4}^*(K_w)\frac{h_{w1}}{B_w}\right] \tag{45}$$

$$L_{w2} = \frac{1}{2}\rho U^2 B_w \left[K_w H^*_{w1}(K_w) \frac{\dot{h}_{w2}}{U} + K_w H^*_{w2}(K_w) \frac{B_w \dot{\alpha}_{w2}}{U} + K_w^2 H^*_{w3}(K_w) \alpha_{w2} + K_w^2 H^*_{w4}(K_w) \frac{h_{w2}}{B_w} \right] \tag{46}$$

$$M_{w2} = \frac{1}{2}\rho U^2 B_w^2 \left[K_w A^*_{w1}(K_w) \frac{\dot{h}_{w2}}{U} + K_w A^*_{w2}(K_w) \frac{B_w \dot{\alpha}_{w2}}{U} + K_w^2 A^*_{w3}(K_w) \alpha_{w2} + K_w^2 A^*_{w4}(K_w) \frac{h_{w2}}{B_w} \right] \tag{47}$$

Reformulation of the aerodynamic forces acting on the wings

$$L_{w1} = \omega_F^2 \pi \rho b_w^2 \left(c^w_{hh} h_{w1} + b_w c^w_{h\alpha} \alpha_{w1} \right) \tag{48}$$

$$M_{w1} = \omega_F^2 \pi \rho b_w^2 \left(b_w c^w_{\alpha h} h_{w1} + b_w^2 c^w_{\alpha\alpha} \alpha_{w1} \right) \tag{49}$$

$$L_{w2} = \omega_F^2 \pi \rho b_w^2 \left(c^w_{hh} h_{w2} + b_w c^w_{h\alpha} \alpha_{w2} \right) \tag{50}$$

$$M_{w2} = \omega_F^2 \pi \rho b_w^2 \left(b_w c^w_{\alpha h} h_{w2} + b_w^2 c^w_{\alpha\alpha} \alpha_{w2} \right) \tag{51}$$

with the coefficients expressed as in Eq. (38).

From Eqs. (13) and (16), it follows that

$$\mathbf{L}^* = \pi\rho \begin{bmatrix} L^*_{11} & L^*_{12} & L^*_{13} & L^*_{14} \\ L^*_{21} & L^*_{22} & L^*_{23} & L^*_{24} \\ L^*_{31} & L^*_{32} & L^*_{33} & L^*_{34} \\ L^*_{41} & L^*_{42} & L^*_{43} & L^*_{44} \end{bmatrix} \tag{52}$$

$$\begin{gathered} L^*_{11} = b^2 c_{hh} + 2 b_w^2 c^w_{hh};\ L^*_{12} = b^3 c_{h\alpha};\\ L^*_{13} = b_w^3 c^w_{h\alpha};\ L^*_{14} = L^*_{13};\\ L^*_{21} = b^3 c_{\alpha h};\ L^*_{22} = b^4 c_{\alpha\alpha} + 2 e^2 b_w^2 c^w_{hh};\\ L^*_{23} = -e b_w^3 c^w_{h\alpha};\ L^*_{24} = -L^*_{23};\\ L^*_{31} = b_w^3 c^w_{\alpha h};\ L^*_{32} = -e b_w^3 c^w_{\alpha h};\ L^*_{33} = b_w^4 c^w_{\alpha\alpha};\ L^*_{34} = 0;\\ L^*_{41} = b_w^3 c^w_{\alpha h};\ L^*_{42} = e b_w^3 c^w_{\alpha h};\ L^*_{43} = 0;\ L^*_{44} = b_w^4 c^w_{\alpha\alpha} \end{gathered} \tag{53}$$

- **CASE 4:** By performing transformations similar to those in **CASE 3**, with

$$\mathbf{L}^* = \pi\rho \begin{bmatrix} L^*_{11} & L^*_{12} & L^*_{13} \\ L^*_{21} & L^*_{22} & L^*_{23} \\ L^*_{31} & L^*_{32} & L^*_{33} \end{bmatrix} \tag{54}$$

In this case, we have

$$\begin{gathered} L^*_{11} = b^2 c_{hh} + b_w^2 c^w_{hh};\ L^*_{12} = b^3 c_{h\alpha} + e b_w^2 c^w_{hh};\ L^*_{13} = b_w^3 c^w_{h\alpha}\\ L^*_{21} = b^3 c_{\alpha h} + e b_w^2 c^w_{hh};\ L^*_{22} = b^4 c_{\alpha\alpha} + e^2 b_w^2 c^w_{hh};\ L^*_{23} = e b_w^3 c^w_{h\alpha};\\ L^*_{31} = b_w^3 c^w_{\alpha h};\ L^*_{32} = e b_w^3 c^w_{\alpha h}; L^*_{33} = b_w^4 c^w_{\alpha\alpha} \end{gathered} \tag{55}$$

References

[1] H.-L. Bui and N.-A. Tran, (2022) *"Multi-objective optimal design of TMDs for increasing critical flutter wind speed of bridges"* **Journal of Wind Engineering and Industrial Aerodynamics 225**: 104992. DOI: 10.1016/j.jweia.2022.104992.

[2] N. Van Khang, A. Seils, T. N. An, N. P. Dien, and N. T. Nghia, (2016) *"An improvement of the step-by-step analysis method for study on passive flutter control of a bridge deck"* **Archive of Applied Mechanics 86**: 557–573. DOI: 10.1007/s00419-015-1046-z.

[3] M. Gu, C. Chang, W. Wu, and H. Xiang, (1998) *"Increase of critical flutter wind speed of long-span bridges using tuned mass dampers"* **Journal of Wind Engineering and Industrial Aerodynamics 73**(2): 111–123. DOI: 10.1016/S0167-6105(97)00282-1.

[4] S.-D. Kwon and K.-S. Park, (2004) *"Suppression of bridge flutter using tuned mass dampers based on robust performance design"* **Journal of Wind Engineering and Industrial Aerodynamics 92**(11): 919–934. DOI: 10.1016/j.jweia.2004.05.006.

[5] F. Ubertini, (2010) *"Prevention of suspension bridge flutter using multiple tuned mass dampers"* **Wind & structures 13**(3): 235–256. DOI: 10.12989/was.2010.13.3.235.

[6] F. Ubertini, G. Comanducci, and S. Laflamme, (2017) *"A parametric study on reliability-based tuned-mass damper design against bridge flutter"* **Journal of Vibration and Control 23**(9): 1518–1534. DOI: 10.1177/1077546315595304.

[7] S. Xue, J. Ko, and Y. L. Xu, (2000) *"Tuned liquid column damper for suppressing pitching motion of structures"* **Engineering Structures 22**(11): 1538–1551. DOI: 10.1016/S0141-0296(99)00099-1.

[8] S. Xue, J. Ko, and Y. L. Xu, (2000) *"Optimum parameters of tuned liquid column damper for suppressing pitching vibration of an undamped structure"* **Journal of sound and vibration 235**(4): 639–653. DOI: 10.1006/jsvi.2000.2947.

[9] J.-C. Wu, Y.-P. Wang, C.-L. Lee, P.-H. Liao, and Y.-H. Chen, (2008) *"Wind-induced interaction of a non-uniform tuned liquid column damper and a structure in pitching motion"* **Engineering Structures *30***(12): 3555–3565. DOI: 10.1016/j.engstruct.2008.05.029.

[10] D. C. d. Arco and Á. C. Aparicio, (1999) *"Improving suspension bridge wind stability with aerodynamic appendages"* **Journal of Structural Engineering *125***(12): 1367–1375. DOI: 10.1061/(ASCE)0733-9445(1999)125:12(1367).

[11] P. Omenzetter, K. Wilde, and Y. Fujino, (2000) *"Suppression of wind-induced instabilities of a long span bridge by a passive deck–flaps control system: Part I: Formulation"* **Journal of Wind Engineering and Industrial Aerodynamics *87***(1): 61–79. DOI: 10.1016/S0167-6105(00)00016-7.

[12] P. Omenzetter, K. Wilde, and Y. Fujino, (2000) *"Suppression of wind-induced instabilities of a long span bridge by a passive deck-flaps control system: Part II: Numerical simulations"* **Journal of Wind Engineering and Industrial Aerodynamics *87***(1): 81–91. DOI: 10.1016/S0167-6105(00)00017-9.

[13] P. Omenzetter, K. Wilde, and Y. Fujino, (2002) *"Study of passive deck-flaps flutter control system on full bridge model. I: theory"* **Journal of Engineering Mechanics *128***(3): 264–279. DOI: 10.1061/(ASCE)0733-9399(2002)128:3(264).

[14] P. Omenzetter, K. Wilde, and Y. Fujino, (2002) *"Study of passive deck-flaps flutter control system on full bridge model. II: Results"* **Journal of engineering mechanics *128***(3): 280–286. DOI: 10.1061/(ASCE)0733-9399(2002)128:3(280).

[15] K. Wilde, Y. Fujino, and T. Kawakami, (1999) *"Analytical and experimental study on passive aerodynamic control of flutter of a bridge deck"* **Journal of Wind Engineering and Industrial Aerodynamics *80***(1-2): 105–119. DOI: 10.1016/S0167-6105(98)00196-2.

[16] T. N. An and N. V. Khang, (2015) *"Increase of critical flutter wind speed of long-span bridges using passive separate control wings"* **16th Asia Pacific Vibration Conference, Vietnam**: 649–653.

[17] U. Starossek and H. Aslan. "Passive control of bridge deck flutter using tuned mass dampers and control surfaces". In: *7th European Conference on Structural Dynamics*, 7–9.

[18] U. Starossek, (2016) *"Eccentric-wing flutter stabilizer for long-span bridges"* **Bridge structures *12***(1-2): 3–9. DOI: 10.3233/BRS-160098.

[19] U. Starossek, T. Ferenczi, and J. Priebe, (2018) *"Eccentric-wing flutter stabilizer for bridges–analysis, tests, design, and costs"* **Engineering structures *172***: 1073–1080. DOI: 10.1016/j.engstruct.2018.06.056.

[20] U. Starossek and R. T. Starossek, (2021) *"Parametric flutter analysis of bridges stabilized with eccentric wings"* **Journal of wind engineering and industrial aerodynamics *211***: 104566. DOI: 10.1016/j.jweia.2021.104566.

[21] U. Starossek and R. T. Starossek, (2021) *"Flutter analysis methods for bridges stabilized with eccentric wings"* **Journal of wind engineering and industrial aerodynamics *219***: 104804. DOI: 10.1016/j.jweia.2021.104804.

[22] S. Phongkumsing, K. Wilde, and Y. Fujino, (2001) *"Analytical study on flutter suppression by eccentric mass method on FEM model of long-span suspension bridge"* **Journal of Wind Engineering and Industrial Aerodynamics *89***(6): 515–534. DOI: 10.1016/S0167-6105(00)00077-5.

[23] D. J. Limebeer, J. M. R. Graham, and X. Zhao, (2011) *"Buffet suppression in long-span suspension bridges"* **Annual Reviews in Control *35***(2): 235–246. DOI: 10.1016/j.arcontrol.2011.10.012.

[24] E. Simiu and R. H. Scanlan. *Wind effects on structures: fundamentals and applications to design*. ***688***. John Wiley New York, 1996.

[25] C. Dyrbye and S. O. Hansen. *Wind loads on structures*. Wiley, 1996.

[26] H. Kobayashi and H. Nagaoka, (1992) *"Active control of flutter of a suspension bridge"* **Journal of Wind Engineering and Industrial Aerodynamics *41***(1-3): 143–151. DOI: 10.1016/0167-6105(92)90402-V.

[27] *Experimentelle Brückenprofile*. Accessed on February 22, 2021. Hamburg University of Technology. URL: https://www.tuhh.de/sdb/brueckenprofile/experimental/experimentelle.html (visited on 02/22/2021).

[28] Y. Fung. *An introduction to the theory of aeroelasticity*. Courier Dover Publications, 2008.

[29] R. L. Bisplinghoff, H. Ashley, and R. L. Halfman. *Aeroelasticity*. Courier Corporation, 2013.

[30] U. Starossek. *Brückendynamik: Winderregte Schwingungen von Seilbrücken*. Springer-Verlag, 2013.

[31] U. Starossek, H. Aslan, and L. Thiesemann, (2009) *"Experimental and numerical identification of flutter derivatives for nine bridge deck sections"* **Wind and Structures *12***(6): 519. DOI: 10.12989/was.2009.12.6.519.

[32] S. S. Rao. *Engineering Optimization Theory and Practice 4th Edition*. John Wiley & Sons, 2009.

[33] R. Fletcher. *Practical methods of optimization*. John Wiley & Sons, 2000.